ADVANCED FUNCTIONAL MATERIALS
www.afm-journal.de

Tuning Magnetic Property and Autophagic Response for Self-Assembled Ni–Co Alloy Nanocrystals

Liang Dong, Yun Liu, Yang Lu, Li Zhang, Na Man, Liang Cao, Kai Ma, Duo An, Jun Lin, Yun-Jun Xu, Wei-Ping Xu, Wen-Bin Wu, Shu-Hong Yu, and Long-Ping Wen**

Induction of autophagy is a common response of cells upon exposure to nanomaterials and represents both a safety concern and an application niche for engineered nanomaterials. Herein, it is reported that the magnetic property and the autophagy-inducing activity for Ni–Co alloy nanocrystal (NC) assemblies can be differentially "tuned" through altering the material composition. A series of Ni–Co alloy NC assemblies, composed of nanoparticles (NPs) with a size of about 30 nm, can be quickly synthesized under microwave irradiation in aqueous solution. A controllable self-assembling effect is observed due to the strong magnetic moment of NPs and external magnetic field. Interestingly, the saturation magnetization (*Ms*) shows a 'roller coaster' effect with varying component molar ratio, while the autophagy-inducing activity and toxicity of these alloy NCs presents an elevated tendency with the increase of nickel component. The autophagic response partly contributes to the observed cellular toxicity of the NC assemblies, as inhibition of autophagy partially but significantly reduces toxicity. Therefore, through tuning the composition of the alloy, optimal Ni–Co NCs satisfying the needs of different applications such as diagnostic imaging (maximum magnetization and low autophagic response) or magnetically-directed cancer cell killing (maximum autophagic response and sufficient magnetization) may be designed and developed.

L. Dong, Y. Lu, L. Cao, K. Ma, D. An, Y.-J. Xu, Prof. S.-H. Yu
Division of Nanomaterials & Chemistry
Department of Chemistry
National Synchrotron Radiation Laboratory
University of Science and Technology of China
Hefei 230026, P. R. China
E-mail: shyu@ustc.edu.cn

Y. Liu, L. Zhang, N. Man, J. Lin, Dr. Y.-J. Xu, Dr. W.-B. Wu, Prof. L.-P. Wen
Hefei National Laboratory for Physical Sciences at the Microscale
School of Life Sciences
University of Science and Technology of China
Hefei 230027, P. R. China
E-mail: lpwen@ustc.edu.cn

Dr. L. Zhang
Department of Urology
the First Affiliated Hospital of Anhui Medical University
and Institute of Urology
Anhui Medical University
Hefei 230022, P. R. China

Dr. Y.-J. Xu, Dr. W.-P. Xu
Anhui Provincial Hospital
Hefei, 230001, P. R. China

DOI: 10.1002/adfm.201203767

1. Introduction

In a wide range of minuscule structures, magnetic nanomaterials have become the focus of intensive research because of their promising applications in biotechnologies,[1] such as manipulation of biological entities,[2] magnetic resonance imaging (MRI),[3,4] biosensing,[5] theranostic,[6,7] drug delivery,[8] gene therapy,[9,10] hyperthermia,[11,12] and cancer treatment.[13,14] In particular, magnetic nanoassemblies provides more controllable behavior than individual NPs in these bio-application in virtue of their more sensitive magnetic response, enhancement of the magnetic properties, and increased multivalent interaction.[2,15] Ni–Co alloys, novel magnetic nanomaterials, are being actively investigated both for their application and chemical synthesis. The Ni–Co alloy nanorings and magnetic-optical nanocomposites were previously confirmed to be outstanding magnetic resonance imaging agents.[16,17] In comparison with generally used iron oxide NCs, this alloy presents more advantages considering its ability to enhance the signal intensity. Since the MRI possesses the characteristics of non-invasive targeting and non-ionizing radiation, the Ni–Co alloy is of great use as a new imaging agent for clinical diagnosis. Furthermore, Ni–Co alloys may also show great prospects in other biologic and clinical fields. However, there are still two main challenges ahead: i) improve the magnetic performance and ii) investigate the detailed biologic effects. For the first challenge, the research on the self-assembling effect is obviously significant. As to the second one, the uncertainty of the biological effects of the Ni–Co alloy functioned at cellular level leads to the necessity of further relevant investigation. High responses in cellular behavior originated from magnetics nanoparticles (MNPs) were observed lately, such as mediate mechanical tension in cells,[18] control apoptosis cell signalling,[19] and so on. The interactions between nanoparticles and cells are proved to be more complex and important, especially the influences of the nanoparticles induced on cells.[20] It has been reported that nanoparticles enter cells through active interaction with celluar mechanisms, for instance, endocytosis.[21] "Protein corona"[22,23] and "cell vision"[24,25] are two main theories that deeply explain the mechanism of the recognization and interaction between nanoparticles and cells.

Autophagy, a highly regulated intracellular process, has become the world matter of concern as a vital cell biology effect in the recent years.[26–28] During this process, a unique membrane sequesters cytoplasmic constituents calls autophagosome, which is of double membrane-bound structure, fuses with lysosome to form autolysosome. Finally, the engulfed cytoplasmic constituents can be degraded by lysosomal enzymes, so that the cell can maintain macromolecular synthesis and energy production.[29,30] Therefore, autophagy is a dynamic and complicated process that can be modulated at various steps, either positively or negatively.[31,32] Recently, a variety of nanomaterials have been reported as a new class of autophagy-inducers, such as quantum dots,[33] rare-earth oxides,[34,35] poly(amidoamine) (PAMAM) nanoparticles,[36] carbon nanotube,[37] fullerene,[38,39] gold and iron oxide nanoparticles.[40–42] The autophagic effect induced by these nanomaterials is frequently disruptive and detrimental to the cell fate.[34–36,42] Therefore, the elicited autophagy may stand for a potential safety concern for the in vivo bio-application of nanomaterials and should be avoided often. But, for certain therapeutic applications, such as cancer therapy, the capacity to induce pro-death autophagy becomes a desirable feature (at least to the targeted cells) and may be purposely exploited dramatically.[39,43,44]

Herein, we report the microwave-assisted synthesis of Ni–Co magnetic alloy NCs with different assembled structures in aqueous solution. Ni–Co alloy NCs with varying molar ratio of Ni/Co from pure nickel, 9:1 to 5:5 via thermal decomposition of nickel and cobalt metal organic compound, can be selectively prepared. In addition, the toxicity and autophagic response induced by Ni_8Co_2, Ni_7Co_3, and Ni_6Co_4 have been investigated systematically. Importantly, the relationship among magnetism, toxicity, and autophagy caused by Ni–Co alloy NCs is firstly reported, indicating a new approach to tune the Ni/Co portion of the alloy with proper magnetism and autophagic response to meet the various requirements of biomedical applications.

2. Results and Discussion

2.1. Synthesis and Identification of Magnetic Ni–Co alloy NCs

For synthesis of alloy nanoparticles, strong reducing agents, such as hydrazine[45] and $NaBH_4$,[10] are frequently used to reduce Ni^{2+} and Co^{2+} easily from their respective inorganic salts. It has been reported that both Ni^{2+} and Co^{2+} can be reduced simultaneously to form homogeneous Ni–Co alloys by classic reduction reaction in aqueous media[45] and even electrochemical method.[46] When microwave irradiation and hydrothermal reaction were used for the preparation of micro- and nanoscale Ni–Co alloy structures, high temperature was not necessary for the thermal decomposition of organometallic precursors. Besides, microemulsion synthesis,[47,48] sol-gel routes,[49] and polyol methods[50] have been widely used for synthesis of metal alloy NPs. Nonetheless, most of the reported research works are mainly on the basis of non-aqueous synthesis using oleic acid or oleylamine.[51] The existence of hydrophobic capping agents usually makes it inconvenient to dissolve the obtained products in water and further greatly limits their bio-applications. Therefore, to prepare high-quality Ni–Co alloy NCs via aqueous synthesis and to study their biological effects are the main tasks.

Microwave-enhanced chemistry is gaining wide acceptance in many types of reactions.[52] Compared with conventional approaches, such as hydrothermal reactions in autoclave, microwave-assisted synthesis can save more time and offer more parameters, such as power, pressure, heating rate, and so on,[53,54] then realizing a reaction with regular monitoring and an alternative heating mode.[55]

In this work, the magnetic Ni–Co alloy NCs were prepared via microwave irradiation method with varying molar ratio of Ni/Co from pure nickel, 9:1 to 5:5. The trend of self-assembly is similar to what we observed in hydrothermal process.[16] Very importantly, the reaction time was greatly shortened to only two minutes, and the high-speed synthesis is of great value in the preparation of functional nanomaterials. Pure Ni NPs and Ni–Co alloy NCs are well stabilized due to the coating of poly(vinylpyrrolidone) (PVP).

The crystalline phase of Ni–Co alloy NCs was identified by powder X-ray diffraction (XRD) analysis. The XRD pattern of Ni_7Co_3 indicates that Ni–Co alloy formed because all the peaks are located between those of pure nickel and pure cobalt (see Supporting Information, Figure S1).[16,56]

Scanning electron microscopy (SEM) and transmission electron microscopy (TEM) images show that the nanostructures of Ni–Co alloy are composed of NCs with an average diameter of about 30 nm as shown in **Figures 1**,**2**. The Ni–Co alloy NCs tend to be self-assembled in aqueous solution, and this effect is strongly dependent on the molar ratio of Ni–Co. Firstly, pure Ni NPs are monodispersed. Secondly, with the decrease of nickel component, Ni–Co alloy NCs with the molar ratio of 9:1 and 8:2 are in a form of long nanochains. When the molar ratio of nickel is reduced to 70%, the self-assembled trend is very much enhanced and the majority of Ni_7Co_3 NCs are nanorings, while others are nanochains with high radian. Finally, the assembly

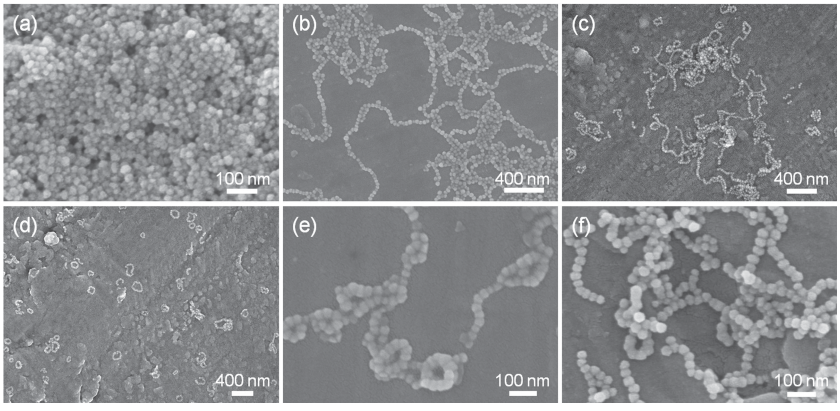

Figure 1. SEM images of Ni–Co alloy NCs with varying Ni/Co ratio from pure nickel, 9:1 to 5:5. a) Ni, b) Ni_9Co_1, c) Ni_8Co_2, d) Ni_7Co_3, e) Ni_6Co_4, f) Ni_5Co_5.

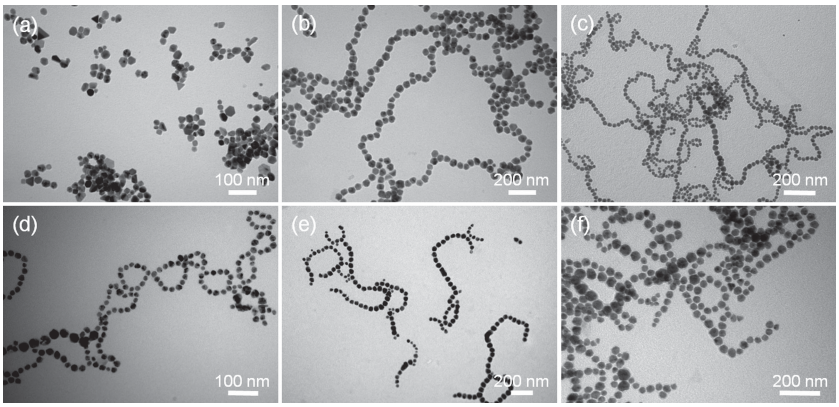

Figure 2. TEM images of Ni–Co alloy NCs with varying Ni/Co ratio from pure nickel, 9:1 to 5:5. a) Ni, b) Ni_9Co_1, c) Ni_8Co_2, d) Ni_7Co_3, e) Ni_6Co_4, f) Ni_5Co_5.

trend decreases and only short nanochains are formed when the molar ratio is reduced to 6:4 and 5:5, which is shown by SEM and TEM images.

2.2 Self-Assembly and Magnetic Property of Ni–Co Alloy NCs

Much attention has been paid to the research of magnetic alloy material owing to their higher saturation magnetization, high magnetic anisotropy, chemical stability,[57,58] and multiple-pose applications.[15,59] To nickel NPs, cobalt NPs, and Ni–Co alloy, strong dipole–dipole magnetic interactions, originated from NPs themselves[16] or magnetic field-induced,[60] are the common and the major driving force of the self-assembly. Various shapes, such as chain,[45] wire,[61] ring,[16,17,62] cage,[63] tube,[64] needle-like,[48] bowl-like,[65] hollow spheres,[66] and core-shell NPs[51] were obtained in different experiments.

The molar ratio of nickel and cobalt sources was varied to investigate the self-assembly phenomena. It is interesting that NPs would not connect with each other at the beginning when pure nickel NPs are formed. While we increase the concentration of cobalt source, the self-assembly trend becomes stronger, and then most of NCs tend to connect with each other and form bracelet-like nanorings when the molar ratio of Ni/Co reaches 7:3. However, when we keep on increasing the concentration of cobalt source, the nanorings begin to break and form nanochains.

As we know, the self-assembly tendency could be influenced by magnetism, surfactant, and the sizes of magnetic NPs. Since all the NPs possessed almost the same diameter (30 nm) and the mass of the surfactant (PVP) was constant in the synthesis, we could exclude possible influence of surfactant and the sizes of NPs. The difference of magnitude of magnetic moment should be responsible for the variety of self-assembly phenomena of different molar ratio of Ni–Co NCs.

Magnetic NPs with different sizes may possess different magnetic status (see Supporting Information, Figure S2). Ni–Co alloy is a conventional ferromagnetic material with multimagnetic domains when the size of the NP is bigger than 50 nm.[67] With the size of NPs decreasing, the domain wall disappears and NPs become single magnetic domain particles, which have a stronger magnetic moment, because the demagnetizing energy becomes smaller than the energy of domain wall.[68] When the size keeps decreasing to less than 10 nm, the energy of thermal motion of magnets over weighs the demagnetizing energy so that NPs become superparamagnetic, which means the direction of each magnet is totally random and can freely rotate independently of the motion.[69]

Considering that our alloy NPs are in the range of single magnetic domain, what is discussed below is mainly based on single magnetic domain Ni–Co NPs. To be accompanied by the spontaneous magnetization taken place in Ni–Co alloy NCs, each NP has its magnetic moment that can be considered as a mini-magnet. NPs with different magnetic pole will attract each other and form a close connection. The stronger the magnetism of alloy is, the stronger the magnetic dipolar interaction is, causing NPs to assemble easily.[70] Conversely, the phenomenon of self-assembly is not obvious: if the magnetism of alloy is smaller, NPs are inclined to disperse in solution.[71,72] Therefore, the molar ratio of nickel and cobalt could determine the self-assembly tendency by affecting the magnetic strength of NPs.

Hence, the trend of self-assembly in different molar ratio of nickel and cobalt is mainly related to the magnetism of alloy NCs, which is in direct proportion to saturation magnetization (*Ms*) to the whole synthetic product. The magnetic properties of Ni–Co alloy NCs have been measured by a superconducting quantum interference device (SQUID) as shown in **Figure 3**.

The field-dependent magnetization (*M–H*) loop shows that while the composition of nickel decreases, the *Ms* increases firstly and then decreases, and it reaches a maximum at the ratio of Ni_7Co_3. When the content of nickel is more than 70%, Ms tends to be more stable, which is embodied in the quasi-overlap between Ni_9Co_1 and Ni_8Co_2. The change trend of *Ms*

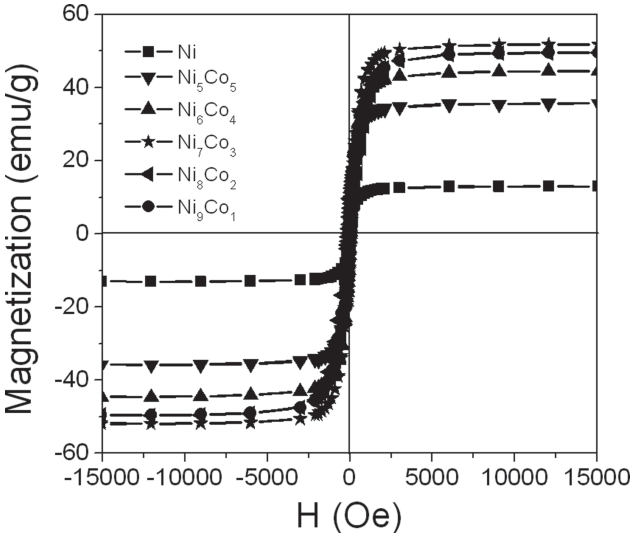

Figure 3. The M–H loops for as-synthesized Ni–Co alloy NCs at 300 K.

of different molar ratio of Ni–Co alloy NCs coincides with that of observed self-assembly tendency, which presents an effect similar to a "roller coaster" as a result of the reduction of nickel and the increase of the cobalt. Because the *M*s of the nanomaterial is the integrated effect of magnetic moment of every NP,[73] the amount of *M*s account for the magnitude of the magnetic moment of each NP towards the homogeneous dimension nanomaterial.[74,75] We could come to the conclusion that the self-assembly tendency is mainly determined by the magnetic moment of Ni–Co alloy, which is also the reason for the changes of self-assembling effect.

Based on sufficient evidences including SEM and TEM images and *M*–*H* curves, the mechanism of the self-assembled effect has been discussed in detail, and a clear explain was given. Above all, Ni–Co NCs were crystallized in the solution. Since nickel and cobalt are classic ferromagnetic materials and have spontaneous magnetization,[76] every Ni–Co NC has a respective magnetic moment. When it comes to the magnetic moment of NPs, the self-assembly tendency is driven by the dipole–dipole interaction of single magnetic domain of Ni–Co alloy NPs, which competes with nondirectional thermal motion at close quarters. When thermal motion exceeds magnetic dipolar interactions, 30 nm NPs are monodisperse.[77] The energy of thermal motion remains the same due to the uniform mass of different composition of Ni–Co alloy NCs. When the magnetic moments of NCs increase, magnetic dipolar interactions will overweight the thermal motion, so that a large number of short nanochains are firstly formed due to the drive of the magnetic dipole–dipole interaction between nearby NCs.

Additionally, the influence of external magnetic field was discussed. It is known that the microwave is generated by the oscillation of electronic–magnetic field, so that the external magnetic field, which is regarded as the drive to form high-radian nanochains rather than flux-closure nanorings is unavoidable in microwave synthesis. In the presence of the applied external magnetic field, most of nanochains formed in the first step will be parallel to the magnetic lines of magnetic force, which will be discussed in details below. Another important part should be mentioned is the self-assembly tendency of Ni_7Co_3 prepared via microwave method. In this case, there are a certain number of NPs forms nanorings rather than nanochains, which is shown in Figures 1d,2d. The reason of this phenomenon is that the magnetic moment of Ni_7Co_3 NCs is strong enough that the magnetostatic field surpasses the external magnetic field so as to form nanochains with high-radian or nanorings.

On the contrary, when it comes to hydrothermal synthesis, where there is no external magnetic field introduced, the short nanochains are in favor of forming nanorings.[16] In this case, magnetostatic direction of short nanochains is disordered without the effect of external magnetic field. The neighboring short nanochains with different magnetostatic directions accidently run into each other in order to decrease the number of magnetic lines of force and magnetostatic energy. There is a high possibility for them to link together by the magnetic dipole–dipole interaction to form nanochains with high-radian and nanorings.

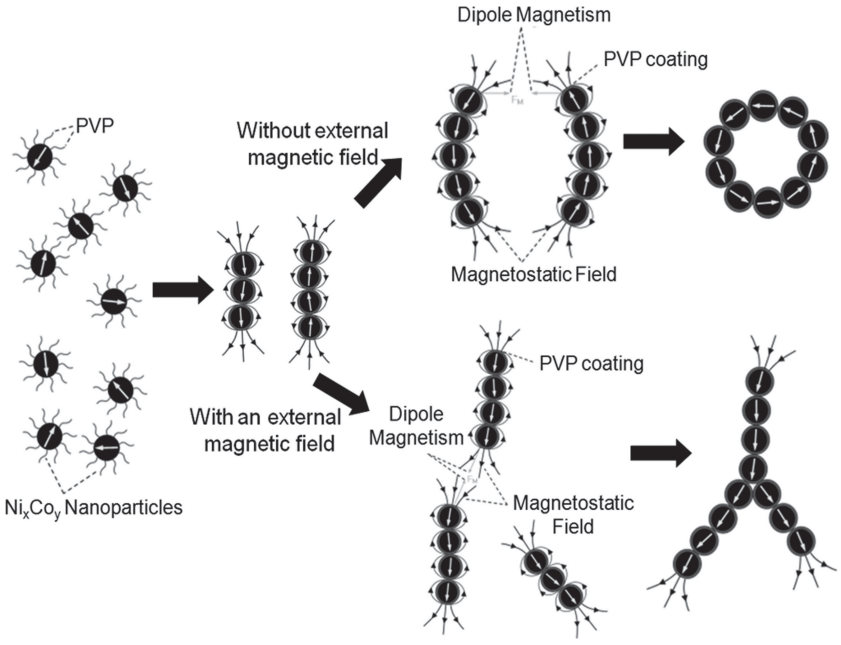

Scheme 1. Scheme of the process of the self-assembly of Ni–Co alloy NCs: a) the formation of Ni–Co NCs encapsulated by a great quantity of surfactant. b) Without external magnetic field, Ni–Co NCs connect with each other in order to form short nanochains with random magneticaligning. c,d) Without external magnetic field, short nanochains connect each other to form nanorings under the action of magnetic dipolar interaction. e,f) With an external magnetic field, short nanochains assemble into long nanochains that have consistent magnetic aligning.

Based on above results and analysis, the schematic diagram of the self-assembly process is summarized and shown in **Scheme 1**. The single domain NPs can move freely in the solution. On account of the magnetic attractive force, the NPs would connect with each other to form short nanochains firstly. In the absence of external magnetic field, the magnetic moment direction of each nanochain is random, resulting in the formation of nanorings. In contrast, while there is an external magnetic field, just like the condition of microwave synthesis, most of the magnetic moment directions of nanochains would be parallel with the magnetic field, so that short chains would connect and form long chains.

2.3. Toxicity and Autophagy-Inducing Capacity of Ni–Co Alloy NCs

Three kinds of alloy NCs (i.e., Ni_8Co_2, Ni_7Co_3, and Ni_6Co_4) were selected to investigate the biological effects of the Ni–Co alloy. The toxicity of Ni–Co alloys was assessed by 3-(4,5-dimethylthiazol-2-yl)-2,5-diphenyltetrazolium bromide (MTT) assay in two different cell lines, namely, human cervical carcinoma (HeLa) and human lung non-small cell carcinoma (H460). These three materials all induced cytotoxic responses in a dose dependent manner after treatment of

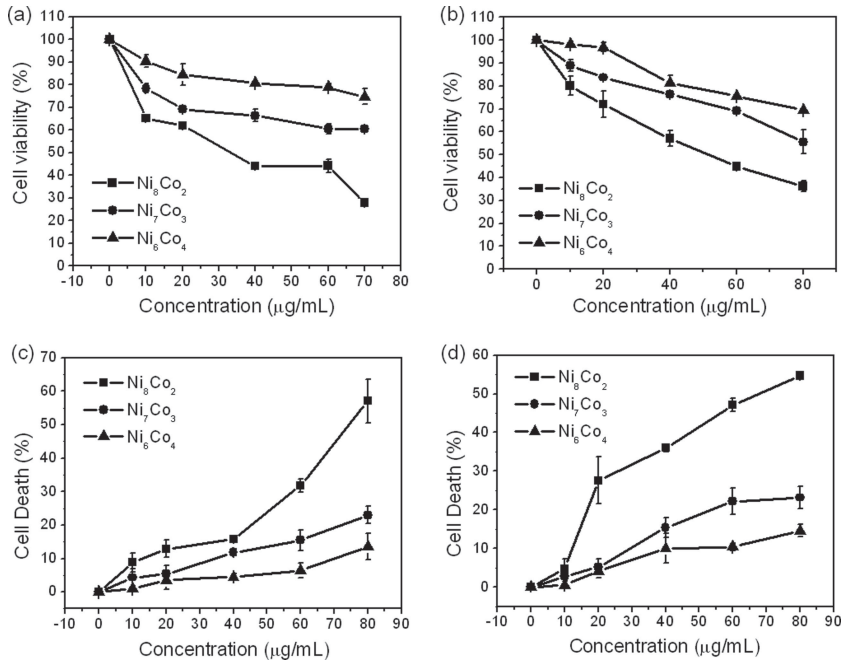

Figure 4. The toxicity of three different Ni–Co alloy NCs. a) HeLa and b) H460 cells were incubated with different concentrations of Ni_8Co_2, Ni_7Co_3, and Ni_6Co_4 for 24 h and the cell viability was detected by the MTT assay. c) HeLa and d) H460 cells were incubated with different concentrations of Ni_8Co_2, Ni_7Co_3, and Ni_6Co_4 for 24 h and the cytotoxicity was detected by the LDH assay. The results are the mean values of triplicates from a representative of three experiments.

HeLa cells separately for 24 h, and the cytotoxicity of the three alloys obviously decreased with the reduction of nickel component. As shown in **Figure 4**a, cell viabilities decreased to about 65.2 ± 0.07%, 78.4 ± 2.08%, 90.5 ± 2.77% by treatment of Ni_8Co_2, Ni_7Co_3, and Ni_6Co_4 at the lower dose of 10 μg mL^{-1}, respectively. While at a relatively higher concentration (70 μg mL^{-1}), these three Ni–Co alloys all impacted the cell states, with the viabilities dropping to about 27.9 ± 1.01%, 60.6 ± 0.76%, and 74.7 ± 3.44%, respectively. Similar results were observed in H460 cells (Figure 4b). Two different assays, namely, the lactate dehydrogenase (LDH) assay (Figure 4c,d) and the 3-(4,5-dimethylthiazol-2-yl)-5(3-carboxymethoxyphenyl)-2-(4-sulfopheny)-2H-tetrazolium (MTS) assay (Supporting Information, Figure 3a,b), revealed the same conclusions. Therefore, these three kinds of Ni–Co alloys all induced cytotoxic effect in a dose-dependent manner, and the toxicity of the alloys presented a downtrend with the reduction of nickel component, rather than the "roller coaster" trend of the magnetism, indicating that the portion of alloy could be modulated for obtaining an optimal Ni–Co alloy with appropriate magnetism and toxicity according to practical requirements.

To assess the autophagy-inducing capacity of Ni–Co alloys, we first established GFP–LC3/HeLa cell line, which stably expressed a fusion protein between green fluorescent protein (GFP) and microtubule-associated light chain 3 (LC3) protein, as LC3 is a standard marker for monitoring autophagy induction. GFP–LC3 protein is normally present diffusely in the cytosol, but it accumulates on the autophagosome membrane when autophagy is elicited, appearing as specific green dots in the cell.[78] Comparing with the dispersed green fluorescence in the untreated control cells, many green punctuate dots were observed in GFP–LC3/HeLa cells after 24 h treatment with Ni_8Co_2, Ni_7Co_3, and Ni_6Co_4, respectively (**Figure 5**a). Ni–Co alloys induced LC3 accumulation in a dose (Figure 5b) and time (Figure S4, Supporting Information) dependent manner. Interestingly, the capacity of inducing LC3 dot formation was different among Ni–Co alloys at the same concentration. Ni_8Co_2 was the strongest while Ni_6Co_4 was the weakest, a result that was consistent with the toxicity of these three alloy NCs. In addition, immunofluorescence was performed to detect the endogenous LC3 protein accumulation. As shown in Figure 5c, the endogenous LC3 protein, revealed as red punctuate dots, was evenly distributed in the untreated cells, but exhibited a punctual pattern in the Ni_8Co_2-treated cells.

LC3 protein conjugates to the membrane of autophagosome and converts from the LC3-I (18 KD) to the LC3-II (16 KD) form when autophagy is up-regulated. Western blot assay clearly showed that all of the three Ni–Co alloys, but not the surfactant PVP used for the production of these alloys, significantly increased the level of LC3-II protein relative to both GAPDH and LC3-I (Figure 5d). It could also be observed that the level of LC3-II is the highest in Ni_8Co_2 treatment cells and the lowest in Ni_6Co_4 treatment cells, while the doses of the three alloys adding into the cells were the same in this assay. These results, together with the LC3 dot formation data and the toxicity data shown above, demonstrated an excellent correlation between autophagy induction and toxicity for the three Ni–Co alloys, as the more toxic alloys induce the more intensive autophagy.

To further confirm that Ni–Co alloys induced autophagy, we performed several additional assays. As shown in Figure S4a, Supporting Information, most of the GFP-LC3 dots observed after Ni–Co treatment could also be stained by monodansylcadaverine (MDC), which stains acidic vesicles specifically. Moreover, co-localization was also observed between GFP–LC3 puncta and the Lyso Tracker Red (LT) staining patterns (Figure S4a, Supporting Information), indicating that many of these GFP–LC3 puncta were probably autolysosomes. TEM directly revealed that cells treated with Ni–Co alloys contained more autophagic vacuoles than the untreated cells (**Figure 6**a). TEM also revealed the presence of many destructive mitochondria in the cells treated with Ni–Co alloys (Figure 6b), suggesting mitophagy. Consistent with this, significant loss of mitochondria membrane potential (MMP) was observed after Ni–Co alloy treatment, and the extent of MMP loss correlated well with their respective autophagy-inducing activity for the three alloys (Figure 6c). In addition, Ni–Co alloy nanocrystal aggregates were frequently observed in the cytosol of cells treated by Ni–Co alloys (Figure 6b). Collectively, the above data lent strong support to the conclusion that Ni–Co alloys induced elevated level of autophagy.

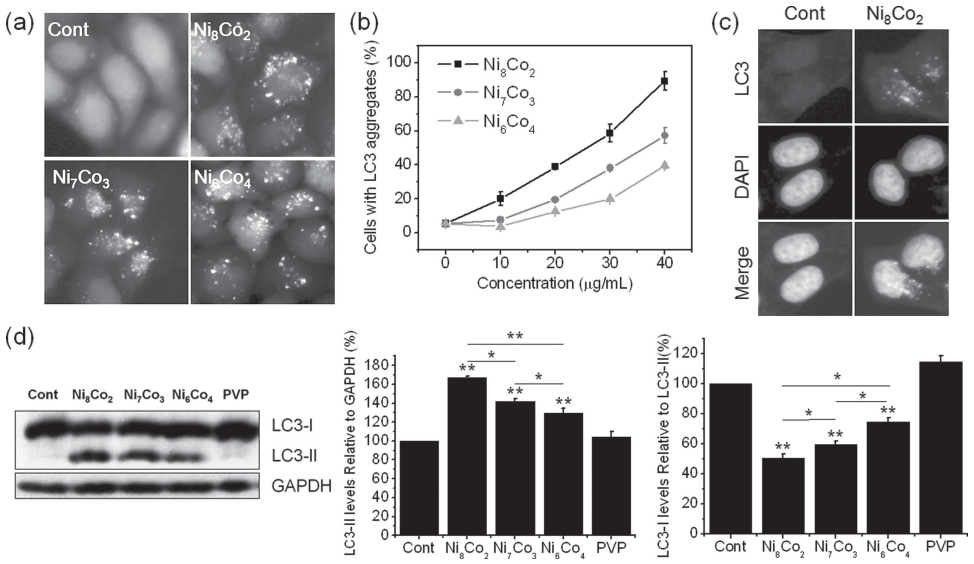

Figure 5. Ni–Co alloy NCs induce LC3 aggregation and conversion in HeLa cells. a) Fluorescent microscopy images of GFP–LC3/HeLa cells treated as following for 24 h. Control: untreated cells. Ni_8Co_2: 20 μg mL^{-1} of Ni_8Co_2. Ni_7Co_3: 30 μg mL^{-1} of Ni_7Co_3. Ni_6Co_4: 40 μg mL^{-1} of Ni_6Co_4. b) Dose-dependent manner of GFP–LC3 dots formation in HeLa–LC3 cells treated with Ni_8Co_2, Ni_7Co_3, and Ni_6Co_4 for 24 h. c) HeLa cells treated with Ni_8Co_2 (20 μg mL^{-1} for 24 h) or untreated (control) were analyzed for endogenous LC3 dots formation with inmmunofluorescent. DAPI represented the nuclear. d) LC3 conversions induced by 40 μg mL^{-1} of Ni_8Co_2, Ni_7Co_3, Ni_6Co_4, and PVP respectively for 24 h and were detected by western blotting using anti-LC3 antibody. LC3-II levels were quantified by densitometric analysis relative to GAPDH and LC3-I levels were also quantified equally relative to LC3-II. (mean ± S.E.M., n = 3, $*p < 0.05$, $**p < 0.01$, compared with the control of each group).

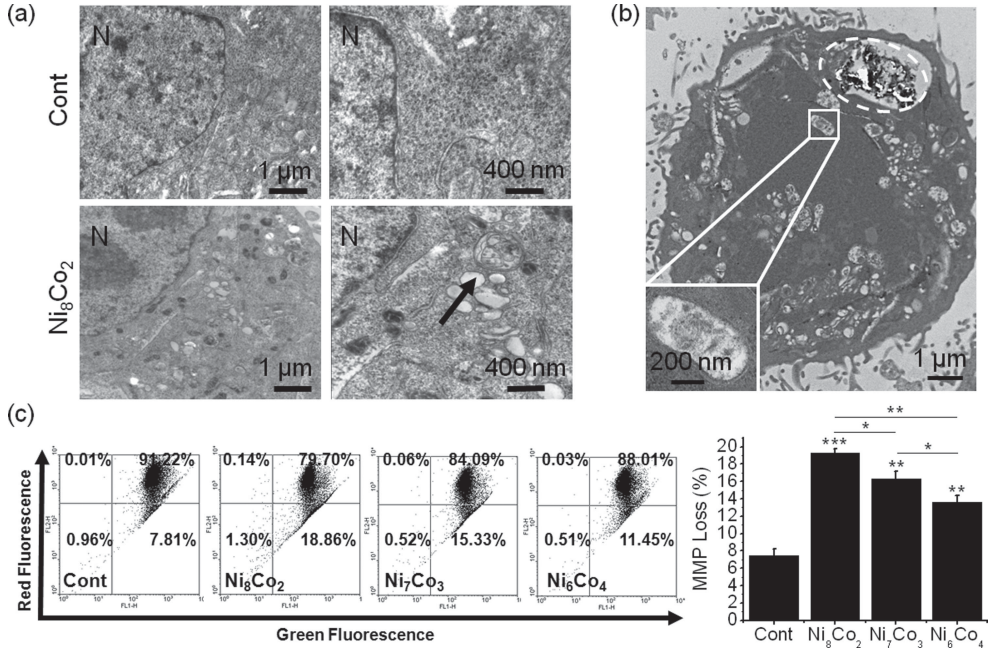

Figure 6. Additional autophagic features induced by Ni–Co alloy NCs in HeLa cells. a) TEM images of HeLa cells untreated (Cont) or treated with Ni_8Co_2 (20 μg mL^{-1}) for 24 h. Right pictures are high-magnification images of left pictures. Typical autophagosome (black arrows) is indicated. b) TEM images indicating the subcellular presence of the magnetic Ni–Co alloy NCs inside Hela cells (white dashed lines). Higher-magnitude images of selected areas with pane displaying a typical destructive mitochondria treated by Ni–Co alloy. c) Effect of Ni–Co alloy NCs on mitochondrial membrane potential (MMP) in Hela cells. Cells were treated with 40 μg mL^{-1} Ni–Co alloy NCs for 24 h, stained with JC-1 and detected with flow cytometry. MMP loss was calculated by the percentage of lower-right quadrant cells. The results are the mean values of triplicates from a representative of three experiments (mean ± SEM, n = 3, $*p < 0.05$, $**p < 0.01$,$*** p < 0.001$, compared to control of each group).

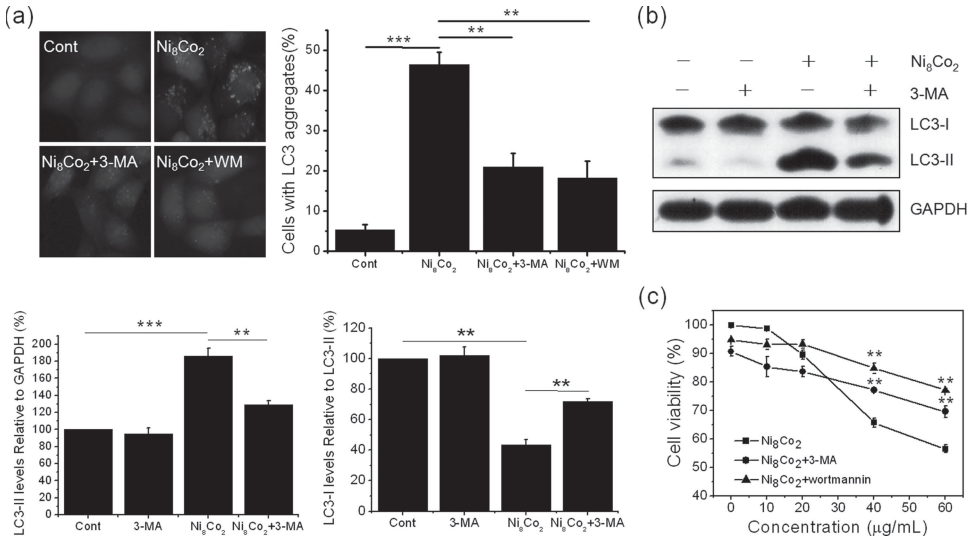

Figure 7. The toxic effect of Ni–Co alloy NCs could be inhibited partially by autophagy inhibition in HeLa cells. a) LC3 dots formation (induced by 20 μg/mL of Ni_8Co_2) could be inhibited by 3-MA (2.5 mM) and wortmannin (500 nM). (Mean ± S.E.M., n = 3, $^{**}p < 0.01$, $^{***}p < 0.001$.) b) LC3 conversion (induced by 40 μg mL^{-1} of Ni_8Co_2) could be inhibited by 3-MA (2.5 mM). LC3-II levels were quantified by densitometric analysis relative to GAPDH and LC3-I levels were also quantified equally relative to LC3-II. (Mean ± S.E.M., n = 3, $^{**}p < 0.01$, $^{***}p < 0.001$.) c) HeLa cells were incubated with different concentrations of Ni_8Co_2 for 24 h with or without pretreatment of 3-MA (2.5 mM) or wortmannin (500 nM) for 2 h and the cell viability was detected by the MTT assay. The results are the mean values of triplicates from a representative of three experiments. (Mean ± S.E.M., n = 3, $^{**}p < 0.01$, compared to only Ni_8Co_2 treatment group at the same concentration.)

2.4. Contribution of Autophagy Induction to the Toxicity of Ni–Co alloys

Induced autophagy may play different roles on the cell fate in different situations and forms the basis for its exploitation in various applications. The observed positive correlation between autophagy induction and toxicity for Ni–Co alloys prompted us to hypothesize that the toxicity of Ni–Co alloys may result, at least partially, from the induction of autophagy. 3-methyladenine (3-MA), a well-known inhibitor of autophagy through regulating the phosphoinositol 3-kinase (PI3K) pathway, partially inhibited the GFP–LC3 dot formation (**Figure 7**a) and LC3 protein conversion (Figure 7b) elicited by Ni–Co alloys. Wortmannin (WM), another common autophagy inhibitor, could also attenuate the LC3 dot formation (Figure 7a) and LC3 protein conversion (data not shown). Consistent with our hypothesis, both 3-MA and wortmannin significantly enhanced HeLa cell viability after Ni–Co alloy treatment at toxic concentrations (Figure 7c). Wortmannin also inhibited about 30.2% of the apoptotic cell death caused by the 24 h treatment of Ni_8Co_2 at 40 μg mL^{-1} concentration, as assessed by Annexin V-FITC staining (**Figure 8**a). This inhibitory effect on apoptotic cell death was presumably the major contributing factor for the cell viability enhancement observed for wortmannin (Figure 7c). On the other hand, Z-VAD, the general inhibitor of caspases, inhibited about 13.4% of the cell viability reduction caused by the same Ni_8Co_2 nanocrystal treatment as revealed by the MTT assay (Figure 8b). As a control, Z-VAD had no effect on the autophagy induced by Ni–Co alloys (Supporting Information, Figure S5). Taken together, these results strongly suggested that Ni–Co alloy nanocrystals caused caspase-dependent as well as caspase-independent cell death, and autophagy contributed to both types of cell death as wortmannin was able to inhibit both of them.

2.5. Magnetically-Directed Autophagic and Cancer Cell Killing Effect of Ni–Co Alloy NCs

While the autophagic response induced by Ni–Co alloy NCs is normally an unwanted side effect in diagnostic imaging and thus should be avoided for these applications, it may enhance tumor cell killing and thus may be exploited for cancer therapy. Among the three Ni–Co alloy NCs, we have studied, Ni_8Co_2 exhibited the highest autophagy-inducing activity while having intermediate magnetic property. We thus tested the ability of this material to elicit enhanced autophagic response and cell death in cancer cells under external magnetic targeting. A magnet was fixed under a cell culture plate to form a magnetic environment for cells in about half of per-hole (magnetic region), while the other half (non-magnetic region) of cells were nearly not affected by magnet (**Figure 9**a). After being joined into the cell culture medium, most Ni_8Co_2 alloys were attracted to the magnetic region immediately. After 12 h, excessive autophagy was observed in almost all the cells cultured in magnetic region and most of the cells had died. Conversely, out of magnetic regions, basal level of autophagy and rare cell death occurred (Figure 9b,c). In order to further investigate the effect of Ni–Co alloys under external magnetic field, we detected the level of autophagy and cell death at 0 h, 2 h, 4 h, 6 h, 8 h, and 10 h. As shown in Figure 9d, autophagy level improved conspicuously at 2 h after treatment, which

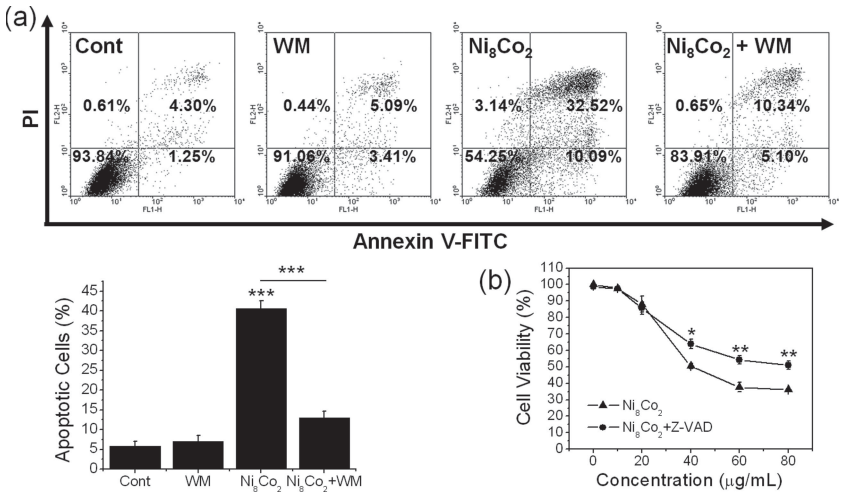

Figure 8. Autophagy contributed to both caspase-dependent and caspase-independent cell death. a) Apoptosis detection was performed by flow cytometric analysis using Annexin-V/PI staining in HeLa cells treated as following. Cont: untreated control; Ni_8Co_2: 40 μg mL^{-1} of Ni_8Co_2 for 24 h; Wortmannin: 500 nM of wortmannin for 24 h; Ni_8Co_2 + wortmannin: 500 nM of wortmannin pre-treatment for 2 h followed by 40 μg mL^{-1} of Ni_8Co_2 for 24 h. The apoptotic level was quantified by the sum of the percentage of early apoptotic (lower-right quadrant) and late apoptotic/necrotic (upper-right quadrant) cells. The results are the mean values of triplicates from a representative of three experiments. (Mean ± S.E.M., n = 3, ***$p < 0.001$, compared to the control group.) b) HeLa cells were incubated with different concentrations of Ni_8Co_2 for 24 h with or without pretreatment of Z-VAD (20 μM) for 0.5 h and the cell viability was detected by the MTT assay. The results are the mean values of triplicates from a representative of three experiments. (Mean ± S.E.M., n = 3, *$p < 0.05$, **$p < 0.01$, compared to only Ni_8Co_2 treatment group at the same concentration.)

was earlier than the apparent occurrence of cell death (at 4 h time point), demonstrating that Ni–Co alloy induced autophagy firstly, then led to cell death. Consistent with our assumption indicated above, these results suggested that autophagy may contribute to the toxicity of Ni–Co alloys. It was also implicated that Ni–Co alloy NCs with considerable autophagic effect and proper magnetism can be employed for cancer treatment.

3. Conclusions

Through the microwave irradiation, we can synthesize the Ni–Co alloy NCs more rapidly in polar solution. With the change of the molar ratio, these alloy NCs display different assembling capacities and effects. The self-assembling trend of the Ni–Co alloy is controllable due to the magnetic moment of NCs and the influence of external magnetic field but not the particle sizes. The *Ms* of these alloy NCs present an effect similar to "roller coaster" as a result of the reduction of nickel component and the increase of cobalt component in the alloy, which is not consistent with the tendency of autophagy-inducing capacity and toxicity. Autophagy

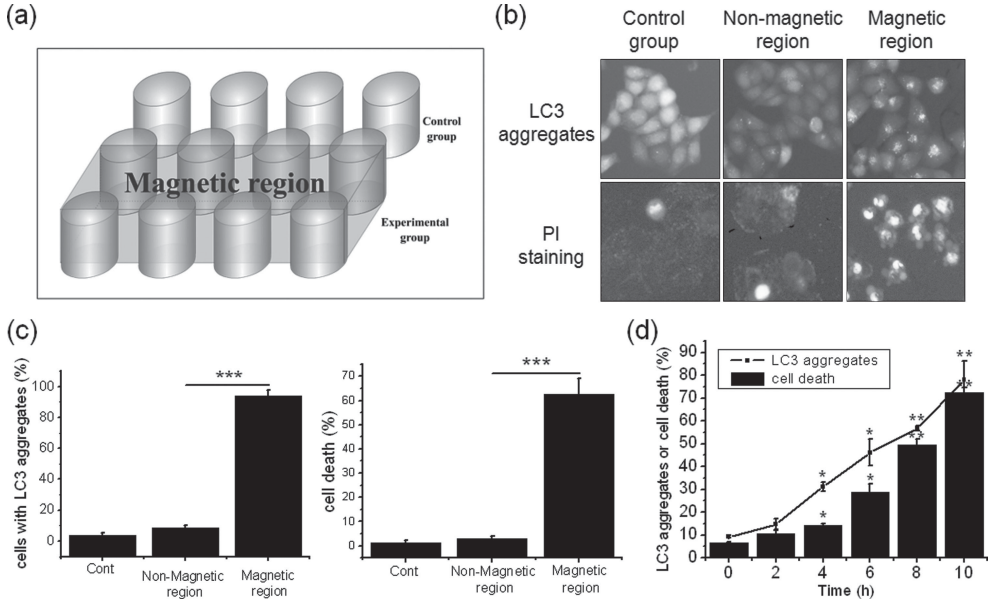

Figure 9. The autophagic and cancer cell killing effect of Ni–Co alloy NCs after magnetic targeting. a) The schematic diagram of magnetic targeting experiment in HeLa–LC3 cells. Experimental group: Hela-LC3 cells incubated with 20 μg mL^{-1} of Ni_8Co_2 for 12 h in the present and absent of magnetic region. (Magnetic region: the blue region. Non-magnetic region: out of the blue region.) Control group: untreated cells incubated without magnetic field. b) The comparison of autophagy and cell death level among magnetic region, non-magnetic region, and control group in Hela–LC3 cells. c) Statistics of autophagy and cell death level among magnetic region, non-magnetic region and control group. Autophagy level was quantified by counting for LC3 aggregates. Cell death was assessed by Hoechst 33342/PI staining and expressed as the percentage of PI-stained cells. (Mean ± S.E.M., n = 3, ***$p < 0.001$.) d) Time course of GFP–LC3 dots formation and cell death level in HeLa–LC3 cells treated with Ni_8Co_2 (20 μg mL^{-1}) under magnetic environment. (Mean ± S.E.M., n = 3,*$p < 0.05$, **$p < 0.01$, compared to 0 h of each group).

has been demonstrated to play a pro-death role on Ni–Co alloy treated cells and autophagy inhibition can partially but significantly reduce the toxicity of Ni–Co alloy. Therefore, our results provide a rational approach for developing Ni–Co alloy NCs optimal for a particular biomedical application by tuning the composition of the alloy. Specifically, Ni–Co alloy NCs with high magnetization and low autophagic effect are ideal for diagnostic imaging, while those with high autophagy-inducing activity and adequate magnetization would be highly desirable for magnetically-directed cancer therapy. By effectively directing the nano-assemblies to the cancer cells through approaches such as molecular targeting, we may also design and develop Ni–Co alloy NCs that exhibit both high magnetization and high autophagy-inducing activity, a material that would enable both cancer diagnostic imaging and therapy in one shot.

4. Experimental Section

Chemicals: The chemicals nickel (II) acetylacetonate ($Ni(acac)_2$, 95%) and cobalt(II) acetylacetonate ($Co(acac)_2$, >99%) were purchased from Alfa Aesar. Triethylene glycol (TREG), polyvinylpyrrolidone (PVP, $M_w \approx 40\,000$) and ethanol were purchased from the Shanghai Reagent Company (P. R. China). All reagents were purchased and used as received without further purification.

Synthesis of Ni–Co Alloy NCs: In a typical synthetic procedure of Ni_7Co_3, a mixture of analytical pure $Co(acac)_2$ (0.0092 g, 3.6×10^{-4} mol), $Ni(acac)_2$ (95%) (0.0227 g, 8.4×10^{-4} mol), and PVP (2.5 g) was added into 15 mL TREG solution. Oil bathing at 135 °C for 30 min with magnetic stirring, the transparent golden yellow solution was quickly transferred into a microwave device (CEM, Discover). The temperature of solution was increased rapidly to 240 °C and held for 2 min; the temperature of solution was then cooled down to 60 °C by an air extracting pump, and a dark black solution formed, which was then diluted with 30 mL ethanol, centrifuged, and ultrasonically dispersed well, washed several times with ethanol to remove ions and possible remnants, and dissolved in ethanol for further characterization. For the synthesis of Ni, the amount of $Ni(acac)_2$ was 1.2×10^{-3} mol. As for the synthesis of Ni_9Co_1, No_8Co_2, Ni_6Co_4, Ni_5Co_5, the corresponding amount of $Ni(acac)_2$ and $Co(acac)_2$ were 1.08×10^{-3} mol, 9.6×10^{-4} mol, 7.2×10^{-4} mol, 6×10^{-4} mol and 1.2×10^{-4} mol, 2.4×10^{-4} mol, 4.8×10^{-4} mol, 6×10^{-4} mol, respectively.

Characterization: The samples were characterized by different analytic techniques. XRD analyses were carried out on a Rigaku D/max-rA X-ray diffractometer with Cu Ka radiation (λ = 1.54178 Å). SEM was performed with a field emission scanning electron microanalyzer (JSM-6700F). TEM was performed on H-800 (Hitachi, Japan) operated at an acceleration voltage of 200 kV. The magnetic properties of the samples were investigated using a superconducting quantum interface device (SQUID) magnetometer (Quantum Design MPMS XL).

Biological Materials: LC3 plasmid was a kind gift from N. Mizushima (The Tokyo Metropolitan Institute of Medical Science, Tokyo, Japan) and Dr. Tamotsu Yoshimori (Osaka University, Japan). LC3 antibody (NB100-2220) was purchased from Novus. HRP-conjugated anti-rabbit antibody (W4011) and HRP-conjugated anti-mouse antibody (W4021) were purchased from Promega. Rhodamine (red) conjugated anti-rabbit antibody (sc-2095) was purchased from Santa Cruz Biotechnology. GAPDH (AB9132) antibody was from Chemcon. DAPI (D8417), 3-methyladenine (3-MA, 08592), monodansylcadaverine (MDC, D4008), wortmannin (W1628) were from Sigma. LysoTracker Red (L7528) was all purchased from Invitrogen. Hoechst 33342 (C1022), Propidium Iodide (PI, ST511), and Z-VAD-FMK (C1202) were from Shanghai Beyotime Company. All cell culture reagents were purchased from Gibco unless otherwise noted.

Cell Culture and Establishment of GFP–LC3/Hela Cells: All cells were grown continuously at 37 °C and 5% CO_2 in Dulbecoo's modified Eagle's medium (DMEM) supplemented with 10% fetal bovine serum (FBS). HeLa cells were transfected with GFP–LC3 plasmid using Lipofectamine 2000 (Invitrogen), according to the manufacturer's protocol. 24 h after transfection, cells were transferred to a new plate and underwent selection in DMEM containing 0.6 mg mL^{-1} of G418 (Promega), with change of medium every three days. Cell colonies exhibiting strong green fluorescence were selected via fluorescent microscopy ten days after transfection and expansion.

Ni-Co Cell Viability Assay-MTT: Cell proliferation analysis was performed by a colorimetric methyl thiazolyl tetrazolium (MTT) assay. Cells were seeded in 96-well plate at a density of 1×10^4 cells/well and incubated for 24 h. Then, cells were treated with Ni–Co alloys at various concentrations. 24 h later, the medium was removed. Cells were washed three times with phosphate buffered saline (PBS) and then 5 mg mL^{-1} MTT were added to each well and incubated for 4 h. The formazan product was dissolved in 200 µL DMSO for 10 min and the absorbance was read at 490 nm with ELx800 Absorbance Microplate Reader (BioTek Instruments, USA).

Cytotoxicity Assay-LDH: Cells were plated at a density of 1×10^4 cells/well in a 96-well plate and allowed to adhere overnight. Cells were then exposed to Ni–Co alloys with various concentrations and incubated for 24 h. LDH analysis was carried out according to the manufacturer's instructions of LDH Cytotoxicity Assay Kit (Beyotime, Shanghai, China. C0017). The absorbance of each well was read at 490 nm with ELx800 Absorbance Microplate Reader (BioTek Instruments, USA).

Cell Viability Assay-MTS: Cell proliferation analysis was performed by colorimetric methyl thiazolyl sulfophenyl (MTS) assay using MTS Cell Proliferation and Cytotoxicity Detection Kit (BestBio, Shanghai, China. 4204). Cells were seeded at a density of 1×10^4 cells/well in a 96-well plate. After incubation for 24 h, different concentrations of Ni–Co alloys were added into cells and incubated for another 24 h. Then, cell medium was removed and cells were washed with PBS for three times. MTS were added into the cells according to the manufacturer's instructions and incubated for 1–2 h. The absorbance of each well was read at 490 nm with ELx800 Absorbance Microplate Reader (BioTek Instruments, USA).

GFP–LC3 Dot Formation Assay: HeLa-LC3 cells were observed 24 h after treatment with Ni–Co alloys under fluorescent microscopy. GFP–LC3 dot formation was quantified by counting 300 cells and expressed as the ratio between the number of cells with at least five GFP–LC3 dots and the number of cells with green fluorescence (essentially 100% for our cells stably expressing GFP–LC3). The assays were independently performed three times.

Autophagic Marker Dye Staining: GFP–LC3/HeLa cells, after treatment with Ni–Co alloys for 24 h, were treated for 15 min with 10 µM MDC and 75 nM LysoTracker Red (LT). After being washed for three times with PBS, cells were examined under fluorescence microscopy (Olympus IX71, Tokyo, Japan).

Western Blot Analysis: Cells treated with various Ni–Co alloys were incubated for 24 h. After cells were collected and lysed, certain proteins were separated on a 15% SDS/PAGE gel and transferred to a nitrocellulose membrane (GE Healthcare Life Sciences) and then blocked with TBST (0.1% Tween) containing 5% nonfat dry milk. The nitrocellulose membrane was incubated for 2 h at room temperature or overnight at 4 °C with primary antibodies at appropriate dilutions and washed six times with TBST (0.1% Tween) and then incubated with HRP-conjugated secondary antibodies at a 1:10 000 dilution for 1 h. Immunolabeling was visualized using an enhanced chemiluminescence (ECL) kit. GAPDH was used as a loading control and was detected using anti-GAPDH antibody.

Immunofluorescence: Cells treated with Ni–Co alloys were washed with PBS and fixed by 4% paraformaldehyde (PFA) in PBS for 5 min at room temperature. The cells were permeabilized with 0.1% TritonX-100 for another 5 min at RT and blocked by 2% fetal bovine serum (FBS) for 1 h. Then the cells were incubated 4 h at RT with LC3 antibody following by an incubation with rhodamine (red) conjugated secondary antibody for 2.5 h. Nucleus were stained with DAPI for 5 min. Finally, the cells were observed under fluorescence microscope (Olympus IX71, Tokyo, Japan).

Electron Microscopy: GFP–LC3/HeLa cells were grown in the 24-well plates and either untreated or treated with Ni–Co alloys for 24 h. After being harvested, cells were fixed in 0.1 M Na-phosphate buffer (pH 7.4) containing 2% glutaraldehyde for 1 h. After ibid in 1% OsO_4 at room temperature for 60 min, cells were dehydrated with a graded series of ethanol, and embedded in epoxy resin. Areas containing cells were block mounted and cut into ultrathin sections. The sections were stained with uranyl acetate and lead citrate and examined with a transmission electron microscope (JEOL-1230, Tokyo, Japan).

Mitochondrial Membrane Potential (MMP) Detection: The changes of mitochondrial membrane potential is assessed by lipophilic cationic probe JC-1 using Mitochondrial Membrane Potential Detection Kit (Beyotime, Shanghai, China. C2006). The JC-1 dye enters the mitochondria, aggregates, and fluoresces red when the mitochondria is normal, while it can no longer accumulate within the mitochondria and fluoresces green if the mitochondrial membrane potential collapses. Briefly, HeLa cells were seeded in 6-well plates and incubated with Ni–Co alloy for 24 h. Then, cells were stained with JC-1 for 20 min in 37 °C, 5% CO_2, washed for twice and instantly detected by flow cytometry at 488 nm excitation, and 530 nm (JC-1 monomers), 590 nm (JC-1 aggregates) emission. Frequency plots represented the percentage of the mitochondria stained green (loss membrane potential) and red (normal membrane potential).

Apoptosis Assay: Apoptosis detection was performed with the Annexin V-FITC Apoptosis Detection Kit (BestBio, Shanghai, China. 401005). Briefly, cells were collected and washed with ice-cold PBS for twice and then resuspended in 400 μL of binding buffer. 5 μL of Annexin V stock solution was added to the cells and incubated for 15 min at 4 °C. The cells were then further incubated with 10 μL propidium iodide (PI) for 5 min at 4 °C and then were immediately analyzed by FACS. Approximately 1×10^4 cells were analyzed in each of the samples.

Cell Death Assay: For cell death assay, cells treated with Ni–Co alloys were stained with Hoechst 33342 (10 mM) and PI (10 mM) for 15 min, washed with PBS for three times and then examined under fluorescence microscopy. Cell death was quantified by counting for 300 cells and the results were expressed by the ratio of PI positive cells to total cells (Hoechst positive cells). The assays were independently performed three times.

Statistical Analysis: All data were expressed as mean ± S.E.M. and analyzed by two-tailed Student's t-tests.

Supporting Information

Supporting Information is available from the Wiley Online Library or from the author. Available are: XRD, schematic illustration of magnetic domain, cell viability assay (MTS), co-localization between GFP-LC3 aggregates and monodansylcadaverine (MDC) or LysoTracker (LT), time course effect of autophagy, the effect of caspase-dependent apoptosis inhibition on autophagy.

Acknowledgements

L. Dong and Y. Liu contributed equally to this work. S.H.Y. and L.P.W. acknowledge the funding support from the National Basic Research Program of China (Grants 2010CB934700, 2007CB935800, 2010CB912804), the National Natural Science Foundation of China (Grants 91022032, 91227103, 21061160492, J1030412, 30721002, 31071211, 30830036, 31170966, 31101020), the Chinese Academy of Sciences (Grants KJZD-EW-M01-1, KSCX2-YW-R-139), International Science & Technology Cooperation Program of China (Grant 2010DFA41170), the Principal Investigator Award by the National Synchrotron Radiation Laboratory at USTC, Scientific and Technological Major Special Project (2009ZX09103-650), and the Fundamental Research Funds for the Central Universities (WK2070000008, WK2060190016). The authors also thank Dr. Noboru Mizushima (Tokyo Medical and Dental University, Japan) and Dr. Tamotsu Yoshimori (Osaka University, Japan) for providing the LC3 plasmid, and thank Dr. Wen Hu (Anhui Provincial Hospital, China) for his support for TEM study, and Jiying Zhao, Jing Li, Cong Sui, Huai-Ling Gao, Jing Xu for their support in this work.

Received: December 19, 2012
Published online: June 25, 2013

[1] A. H. Lu, E. L. Salabas, F. Schuth, *Angew. Chem. Int. Ed.* **2007**, *46*, 1222.
[2] Y. Pan, X. Du, F. Zhao, B. Xu, *Chem. Soc. Rev.* **2012**, *41*, 2912.
[3] D. S. Ling, W. Park, Y. I. Park, N. Lee, F. Y. Li, C. Song, S. G. Yang, S. H. Choi, K. Na, T. Hyeon *Angew. Chem. Int. Ed.* **2011**, *50*, 11360.
[4] R. R. Qiao, C. H. Yang, M. Y. Gao, *J. Mater. Chem.* **2009**, *19*, 6274.
[5] S. Y. Park, H. Handa, A. Sandhu, *Nano Lett.* **2010**, *10*, 446.
[6] D. Ho, X. L. Sun, S. H. Sun, *Acc. Chem. Res.* **2011**, *44*, 875.
[7] X. Xue, F. Wang, X. Liu, *J. Mater. Chem.* **2011**, *21*, 13107.
[8] M. Arruebo, R. Fernández-Pacheco, M. R. Ibarra, J. Santamaría, *Nano Today* **2007**, *2*, 22.
[9] J. Dobson, *Gene Ther.* **2006**, *13*, 283.
[10] Y. Lu, Y. Zhao, L. Yu, L. Dong, C. Shi, M. J. Hu, Y. J. Xu, L. P. Wen, S. H. Yu, *Adv. Mater.* **2010**, *22*, 1407.
[11] A. K. Gupta, M. Gupta, *Biomaterials* **2005**, *26*, 3995.
[12] J. P. Fortin, C. Wilhelm, J. Servais, C. Ménager, J. C. Bacri, F. Gazeau, *J. Am. Chem. Soc.* **2007**, *129*, 2628.
[13] N. Tran, T. J. Webster, *J. Mater. Chem.* **2010**, *20*, 8760.
[14] J. H. Lee, J. T. Jang, J. S. Choi, S. H. Moon, S. H. Noh, J. W. Kim, J. G. Kimm, I. S. Kim, K. I. Park, J. Cheon, *Nat. Nanotechnol.* **2011**, *6*, 418.
[15] Y. Lu, L. Dong, L. C. Zhang, Y. D. Su, S. H. Yu, *Nano Today* **2012**, *7*, 297.
[16] M. J. Hu, Y. Lu, S. Zhang, S. R. Guo, B. Lin, M. Zhang, S. H. Yu, *J. Am. Chem. Soc.* **2008**, *130*, 11606.
[17] Y. Lu, C. Shi, M. J. Hu, Y. J. Xu, L. Yu, L. P. Wen, Y. Zhao, W. P. Xu, S. H. Yu, *Adv. Funct. Mater.* **2010**, *20*, 3701.
[18] P. Tseng, J. W. Judy, D. Di Carlo, *Nat. Methods* **2012**, *9*, 1113.
[19] M. H. Cho, E. J. Lee, M. Son, J. H. Lee, D. Yoo, J. Kim, S. W. Park, J. S. Shin, J. Cheon *Nat. Mater.* **2012**, *11*, 1038.
[20] S. Laurent, C. Burtea, C. Thirifays, U. O. Hafeli, M. Mahmoudi, *PLoS One* **2012**, *7*, e29997.
[21] A. Lesniak, F. Fenaroli, M. P. Monopoli, C. Åberg, K. A. Dawson, A. Salvati, *ACS Nano* **2012**, *6*, 5845.
[22] M. P. Monopoli, D. Walczyk, A. Campbell, G. Elia, I. Lynch, F. B. Bombelli, K. A. Dawson *J. Am. Chem. Soc.* **2011**, *133*, 2525.
[23] M. Mahmoudi, I. Lynch, M. R. Ejtehadi, M. P. Monopoli, F. B. Bombelli, S. Laurent, *Chem. Rev.* **2011**, *111*, 5610.
[24] M. Mahmoudi, S. N. Saeedi-Eslami, M. A. Shokrgozar, K. Azadmanesh, M. Hassanlou, H. R. Kalhor, C. Burtea, B. Rothen-Rutishauser, S. Laurent, S. Sheibani, H. Vali, *Nanoscale* **2012**, *4*, 5461.
[25] D. Walczyk, F. B. Bombelli, M. P. Monopoli, I. Lynch, K. A. Dawson *J. Am. Chem. Soc.* **2010**, *132*, 5761.
[26] N. Mizushima, B. Levine, A. M. Cuervo, D. J. Klionsky, *Nature* **2008**, *451*, 1069.
[27] A. Kelekar, *Ann. N. Y. Acad. Sci.* **2005**, *1066*, 259.
[28] D. J. Klionsky, *Nat. Rev. Mol. Cell Biol.* **2007**, *8*, 931.
[29] M. Kundu, C. B. Thompson, *Ann. Rev. Pathol.* **2008**, *3*, 427.
[30] N. Mizushima, T. Yoshimori, B. Levine, *Cell* **2010**, *140*, 313.
[31] D. J. Klionsky, H. Abeliovich, P. Agostinis, *Autophagy* **2008**, *4*, 151.
[32] K. H. Baek, J. Park, I. Shin, *Chem. Soc. Rev.* **2012**, *41*, 3245.
[33] O. Seleverstov, O. Zabirnyk, M. Zscharnack, L. Bulavina, M. Nowicki, J. M. Heinrich, M. Yezhelyev, F. Emmrich, R. O'Regan, A. Bader, *Nano Lett.* **2006**, *6*, 2826.

[34] Y. Chen, L. S. Yang, C. Feng, L. P. Wen, *Biochem. Biophys. Res. Commun.* **2005**, *337*, 52.
[35] L. Yu, Y. Lu, N. Man, S. H. Yu, L. P. Wen, *Small* **2009**, *5*, 2784.
[36] C. G. Li, H. L. Liu, Y. Sun, H. L. Wang, F. Guo, S. A. Rao, J. J. Deng, Y. L. Zhang, Y. F. Miao, C. Y. Guo, J. Meng, X. P. Chen, L. M. Li, D. S. Li, H. Y. Xu, H. Wang, B. Li, C. Y. Jiang, *J. Mol. Cell Biol.* **2009**, *1*, 37.
[37] H. L. Liu, Y. L. Zhang, N. Yang, Y. X. Zhang, X. Q. Liu, C. G. Li, Y. Zhao, Y. G. Wang, G. G. Zhang, P. Yang, F. Guo, Y. Sun, C. Y. Jiang, *Cell Death Dis.* **2011**, *2*, 159.
[38] L. Harhaji, A. Isakovic, N. Raicevic, Z. Markovic, B. Todorovic-Markovic, N. Nikolic, S. Vranjes-Djuric, I. Markovic, V. Trajkovic, *Eur. J. Pharmacol* **2007**, *568*, 89.
[39] Q. Zhang, W. J. Yang, N. Man, F. Zheng, Y. Y. Shen, K. J. Sun, Y. Li, L. P. Wen, *Autophagy* **2009**, *5*, 1107.
[40] J. J. Li, D. Hattono, C. N. Ong, B. H. Bay, L. Y. L. Yung, *Biomaterials* **2010**, *31*, 5996.
[41] X. W. Ma, Y. Y. Wu, S. B. Jin, Y. Tian, X. N. Zhang, Y. L. Zhao, L. Yu, X. J. Liang, *ACS Nano* **2011**, *5*, 8629.
[42] M. I. Khan, A. Mohammad, G. Patil, S. A. H. Naqvi, L. K. S. Chauhan, I. Ahmad, *Biomaterials* **2012**, *33*, 1477.
[43] Y. N. Wu, L. X. Yang, X. Y. Shi, I. C. Li, J. M. Biazik, K. R. Ratinac, D. H. Chen, P. Thordarson, D. B. Shieh, F. Braet, *Biomaterials* **2011**, *32*, 4565.
[44] P. F. Wei, L. Zhang, Y. Lu, N. Man, L. P. Wen, *Nanotechnology* **2010**, *21*, 5101.
[45] L. P. Zhu, H. M. Xiao, S. Y. Fu, *Eur. J. Inorg. Chem.* **2007**, *2007*, 3947.
[46] G. Qiao, T. Jing, N. Wang, Y. Gao, X. Zhao, J. Zhou, W. Wang, *Electrochim. Acta* **2005**, *51*, 85.
[47] J. Ahmed, S. Sharma, K. V. Ramanujachary, S. E. Lofland, A. K. Ganguli, *J. Colloid Interf. Sci.* **2009**, *336*, 814.
[48] D. E. Zhang, X. M. Ni, X. J. Zhang, H. G. Zheng, *J. Magn. Magn. Mater.* **2006**, *302*, 290.
[49] G. Mattei, C. de J. Fernández, P. Mazzoldi, C. Sada, G. De, G. Battaglin, C. Sangregorio, D. Gatteschi, *Chem. Mater.* **2002**, *14*, 3440.
[50] O. Jayakumar, H. Salunke, A. Tyagi, *Solid State Commun.* **2009**, *149*, 1769.
[51] T. Yamauchi, Y. Tsukahara, K. Yamada, T. Sakata, Y. Wada, *Chem. Mater.* **2011**, *23*, 75.
[52] M. Baghbanzadeh, L. Carbone, P. D. Cozzoli, C. O. Kappe, *Angew. Chem. Int. Ed.* **2011**, *50*, 11312.
[53] G. R. Patzke, Y. Zhou, R. Kontic, F. Conrad, *Angew. Chem. Int. Ed.* **2011**, *50*, 826.
[54] Y. Lu, L. Zhang, J. Li, Y. D. Su, Y. Liu, Y. J. Xu, L. Dong, H. L. Gao, J. Lin, N. Man, P. F. Wei, W. P. Xu, S. H. Yu, L. P. Wen, *Adv. Funct. Mater.* **2012**, *23*, 1534.
[55] V. P. Mehta, E. V. Van der Eycken, *Chem. Soc. Rev.* **2011**, *40*, 4925.
[56] H. Zhang, T. Yao, Z. H. Sun, Y. Y. Li, Q. H. Liu, F. C. Hu, Z. Y. Pan, B. He, Z. Xie, S. Q. Wei, *J. Phys. Chem. C* **2010**, *114*, 13596.
[57] S. H. Sun *Adv. Mater.* **2006**, *18*, 393.
[58] E. V. Shevchenko, D. V. Talapin, H. Schnablegger, A. Kornowski, Ö. Festin, P. Svedlindh, M. Haase, H. Weller, *J. Am. Chem. Soc.* **2003**, *125*, 9090.
[59] J. H. Gao, G. L. Liang, J. S. Cheung, Y. Pan, Y. Kuang, F. Zhao, B. Zhang, X. Zhang, E. X. Wu, B. Xu, *J. Am. Chem. Soc.* **2008**, *130*, 11828.
[60] M. Wu, G. Liu, M. Li, P. Dai, Y. Ma, L. Zhang, *J. Alloys Compd.* **2010**, *491*, 689.
[61] N. Bagkar, K. Seo, H. Yoon, J. In, Y. Jo, B. Kim, *Chem. Mater.* **2010**, *22*, 1831.
[62] S. L. Tripp, R. E. Dunin-Borkowski, A. Wei, *Angew. Chem. Int. Ed.* **2003**, *42*, 5591.
[63] X. Wang, H. B. Fu, A. D. Peng, T. W. Zhai, Y. Ma, F. L. Yuan, J. N. Yao, *Adv. Mater.* **2009**, *21*, 1636.
[64] L. Guo, C. M. Liu, R. M. Wang, H. B. Xu, Z. Y. Wu, S. H. Yang, *J. Am. Chem. Soc.* **2004**, *126*, 4530.
[65] W. Zhou, L. Lin, D. Zhao, L. Guo, *J. Am. Chem. Soc.* **2011**, *133*, 8389.
[66] X. Wang, F. L. Yuan, P. Hu, L. J. Yu, L. Y. Bai, *J. Phys. Chem. C* **2008**, *112*, 8773.
[67] U. Jeong, X. Teng, Y. Wang, H. Yang, Y. N. Xia, *Adv. Mater.* **2007**, *19*, 33.
[68] R. Danneau, P. Warin, J. Attané, I. Petej, C. Beigné, C. Fermon, O. Klein, A. Marty, F. Ott, Y. Samson, *Phys. Rev. Lett.* **2002**, *88*, 157201.
[69] L. Lopez-Diaz, L. Torres, E. Moro, *Phys. Rev. B* **2002**, *65*, 224406.
[70] J. Y. Ku, D. M. Aruguete, A. P. Alivisatos, P. L. Geissler, *J. Am. Chem. Soc.* **2011**, *133*, 838.
[71] C. T. Yavuz, J. Mayo, W. W. Yu, A. Prakash, J. C. Falkner, S. Yean, L. Cong, H. J. Shipley, A. Kan, M. Tomson, D. Natelson, V. L. Colvin, *Science* **2006**, *314*, 964.
[72] Z. Liu, H. Wang, Q. Lu, G. Du, L. Peng, Y. Du, S. Zhang, K. Yao, *J. Magn. Magn. Mater.* **2004**, *283*, 258.
[73] K. Büscher, C. Helm, C. Gross, G. Glöckl, E. Romanus, W. Weitschies, *Langmuir* **2004**, *20*, 2435.
[74] A. Clogston, B. Matthias, M. Peter, H. Williams, E. Corenzwit, R. Sherwood, *Phys. Rev.* **1962**, *125*, 541.
[75] J. Chen, C. Sorensen, K. Klabunde, G. Hadjipanayis, *Phys. Rev. B* **1995**, *51*, 11527.
[76] M. Kuz'min, *Phys. Rev. Lett.* **2005**, *94*, 107204.
[77] J. Philip, P. Shima, B. Raj, *Nanotechnology* **2008**, *19*, 305706.
[78] Y. Kabeya, N. Mizushima, T. Uero, A. Yamamoto, T. Kirisako, T. Noda, E. Kominami, Y. Ohsumi, T. Yoshimori, *EMBO J.* **2000**, *19*, 5720.